SAND78-8276
Unlimited Release

Natural Convection Heat Transfer From an External Receiver

D. Siebers

Prepared by Sandia Laboratories, Albuquerque, New Mexico 87115 and Livermore, California 94550 for the United States Department of Energy under Contract DE-AC04-76DP00789.

Printed December 1979

Sandia Laboratories
energy report

Issued by Sandia Laboratories, operated for the United States Department of Energy by Sandia Corporation.

NOTICE

SAND78-8276
Unlimited Release
Printed December 1979

NATURAL CONVECTION HEAT TRANSFER FROM AN EXTERNAL RECEIVER

Dennis Siebers
Thermal Sciences Division 8124
Sandia Laboratories, Livermore

ABSTRACT

A numerical solution of turbulent, two-dimensional, natural convection heat transfer for a high temperature, vertical surface is presented in this work. This is relevant to heat transfer from the receiver of a solar central receiver power plant on a calm day (no wind). It is the lower bound of convective loss from an external receiver. Application of wall suction to the receiver surface is also examined as a means of reducing convective loss.

Several conclusions can be drawn from the results. First, natural convection heat transfer caused by high operating temperatures and long vertical surfaces is an important heat loss mechanism from a receiver. Second, heat transfer correlations based on experimental work at much lower temperatures and Grashof numbers ($< 10^{12}$) do not apply to high temperature and high Grashof number ($10^{13} - 10^{14}$) natural convection on a receiver. This model, based on realistic physical assumptions, estimates heat transfer rates 50 to 100 percent higher for temperatures and Grashof numbers in the range of interest than the empirical models developed at lower temperatures and Grashof numbers currently used by many receiver designers. Third, analytically derived correlations based on the assumption of constant properties across a boundary layer are not appropriate for the high temperature natural convection heat transfer on receivers. The model demonstrates that large temperature differences between the wall and free stream significantly effect the heat transfer as a result of the large property variations across the boundary layer. Finally, boundary layer suction results show suction can be used to reduce convective heat loss from a receiver especially

if some of the energy in the air extracted through the wall can be used to preheat the working fluid in the receiver.

In the Appendix an analysis of the economic impact of energy loss from a receiver is presented. It demonstrates the importance of receiver performance with regard to solar central receiver plant cost.

CONTENTS

ILLUSTRATIONS

NOMENCLATURE

a	constant in the relation for turbulent viscosity
$\overline{AC}$	annualized fixed charge
A^+	damping constant in van Driest damping function
b	constant in the relation for turbulent energy dissipation
B	balance of plant capital cost (plant cost less heliostat field cost and receiver cost)
$\overline{BBEC}$	levelized busbar energy cost
c	specific heat of fluid
C	heliostat field cost
CAP	rated plant capacity in kilowatts
CF	ratio of the average load for a year to rated plant capacity.
CI	total capital investment in plant
d	factor for interest charged during construction period on capital investment money.
D	damping function to suppress mixing length in the region immediately adjacent to a wall
$\overline{FL}$	levelized annual fuel cost
g	local gravitational constant to determine free-convection body force
g_c	proportionality constant, Newton's second law
Gr	Grashof number $(g\beta(T_w-T_\infty)x^3/\nu^2)$
i*'	fluctuation in stagnation enthalpy
I	static enthalpy of fluid
I*	stagnation enthalpy of fluid $(I + U^2/2g_c J)$
J	conversion constant, mechanical energy to thermal energy
J_q	diffusion term, turbulent kinetic energy equation
k	thermal conductivity of fluid
KWH	annual energy output of plant in kilowatt hours
ℓ	mixing length

$\dot{m}$	suction rate at the wall
n	receiver efficiency, ratio of energy transferred to working fluid to energy incident on receiver.
Nu	Nusselt number
$\overline{OM}$	levelized annual operations and maintenance cost
P	thermodynamic pressure
Pr	Prandtl number
Pr_t	turbulent Prandtl number ($\varepsilon_M/\varepsilon_H$)
$q^2/2$	turbulent kinetic energy
Q	heat transfer rate
R	radius of curvature of receiver surface
RI	receiver capital cost
Sc_q	turbulent Schmidt number ($\varepsilon_M/\varepsilon_q$)
U	velocity component in x-direction
U_τ	shear velocity $\sqrt{g_c \tau_o/\rho_o}$
u'	fluctuation in U component of velocity
V	velocity component in y-direction
v'	fluctuation in V component of velocity
x	distance along surface
y	distance normal to surface
y^+	dimensionless y distance, $y\ U_\tau/\nu_o$
β	volume coefficient of expansion
δ	boundary layer thickness where $U/U_\infty = 0.99$
ε_H	eddy diffusivity for heat
ε_M	eddy diffusivity for momentum
ε_q	eddy diffusivity for turbulent kinetic energy
κ	Karman constant, mixing length model
λ	outer length scale constant mixing length model
ν	kinematic viscosity of fluid
ρ	density of fluid
τ	combined laminar and turbulent shear stress

Subscripts

bl	boundary layer
m	maximum value
$_{w}^{o}$	wall value
s	wall suction value
∞	free stream value

NATURAL CONVECTION HEAT TRANSFER FROM AN EXTERNAL RECEIVER

Introduction

The solar central receiver concept is being extensively studied as a possible means of supplying large quantities of energy at high temperatures for process heat or for electric power generation needs. The concept is based on a redirection of the incoming collimated solar radiation by a heliostat field onto a focal point on a tower. A receiver located at the focal point absorbs the solar energy and transfers it to a working fluid as thermal energy. The thermal energy is then used for process heat or generating electricity.

Two types of receivers, cavity and external, have been designed. The cavity receiver has an aperture through which the solar energy is directed. The energy is then absorbed on the interior surface. The external receiver has the solar energy absorbing surface on the exterior, directly exposed to the environment.

Efficient absorbtion and transfer of the solar energy to the working fluid by the receiver is critical to the central receiver concept. Plant performance, plant capital cost, and the cost of the energy produced are significantly affected by the receiver efficiency (see Appendix). Therefore, a detailed understanding of the heat transfer processes occurring in the receiver is important. These heat transfer processes include absorption of incoming solar radiation, emission of thermal radiation by the receiver surface to the atmosphere, convection from receiver surface to the atmosphere, convection of energy to the working fluid, and conduction in the receiver walls.

The focus of this work is convective heat transfer from an external receiver to the atmosphere, which represents an energy loss from the receiver.

Preliminary estimations of convective heat loss for current receiver designs indicate that it varies between a few percent at design point conditions (high solar flux, low wind, and lower bound on uncertainty in convective heat transfer), to as much as thirty percent at off-design conditions (low solar flux, high wind, and upper bound on uncertainty in convective heat transfer). The magnitude of energy lost by convection from a receiver depends on receiver operating conditions such as the incident solar flux, the receiver temperature, and the atmospheric wind speed.

Since convection can account for a large part of the energy lost from a receiver, accurate estimations of convective heat losses are necessary. Currently, this is not possible. The turbulent three-dimensional mixed convective flow around a receiver with Grashof numbers based on the height of the receiver from 10^{13} through 10^{14} and with Reynolds numbers based on the width of the receiver from 10^{6} through 10^{7} has not been examined. This is the result of the characteristics of the receiver and the air flow around it that make the problem difficult to examine experimentally or numerically. Some of these characteristics are the high operating temperatures (500 to 1200 C) the large receiver dimensions (10 to 30 m in any direction), the rough surface on the receivers created by tubes welded together to form the heat transfer surface through which the working fluid flows, the three-dimensional nature of the air flow caused by strong bouyant forces and the three-dimensional shape of the receiver, and the turbulence in the free stream and the boundary layer.

Because of the complexity of the overall three-dimensional convection heat transfer from a receiver, a much simpler two-dimensional problem was examined as a first step: turbulent natural convection heat transfer from a high temperature vertical flat surface.† This represents the convective heat transfer from an external receiver on a calm day with no wind, which is the lower bound of convective loss. It is is also related to heat transfer from the large vertical surfaces in cavities.

This report presents a numerical solution that problem and compares it with previous related work. First, the central receiver concept and the

---

†The curvature of the receiver in the cross flow direction can be neglected since the boundary layer thickness is small compared to the radius of curvature ($\delta/R < .01$)

importance and complexity of convection heat transfer from receivers are briefly introduced. This is followed by the physical model, the method of solution, and the results and discussion of the study of turbulent natural convection from a vertical surface. The appendix contains a discussion of the effects of receiver efficiency on the capital cost and the cost of energy produced for a solar power plant.

Model

This section contains a brief description of the mathematical model for high Grashof number, natural convection heat transfer from a vertical plate. The model is a simplified form of the fluid mechanic and heat transfer model presented in Reference 1, which is a document describing the computer code, STAN-5. That code numerically solves two-dimensional internal and external boundary layer flows with variable properties. The reader should refer to Reference 1 for more detailed information on the general physical model which STAN-5 numerically solves and the assumptions used to develop that model.

The following simplified continuity, momentum, and energy equations comprise the two-dimensional model for natural convection from a vertical surface solved with STAN-5:

Continuity,

$$\frac{\partial}{\partial x}(\rho U) + \frac{\partial}{\partial y}(\rho V) = 0 \quad . \tag{1}$$

Momentum,

$$\rho U \frac{\partial U}{\partial x} + \rho V \frac{\partial U}{\partial y} = -g_c \frac{dP}{dx} + \frac{\partial}{\partial y}\left[\mu \frac{\partial U}{\partial y} - \rho \overline{u'v'}\right] - \rho g \quad . \tag{2}$$

Energy,

$$\rho U \frac{\partial I^*}{\partial x} + \rho V \frac{\partial I^*}{\partial y} = \frac{\partial}{\partial y}\left[\frac{k}{c}\frac{\partial I}{\partial y} - \rho \overline{i^* v'} + \frac{\rho \nu}{g_c J}\frac{\partial}{\partial y}\left(\frac{U^2}{2}\right)\right] \tag{3}$$

Derivation of these equations has been presented in several basic texts [2-4] and will not be repeated here.

The boundary conditions for the equations are the following:

$$\begin{aligned} &\text{at } y = 0, \quad U = V = 0 \quad \text{and} \quad I^* = I^*_w; \\ &\text{at } y \to \infty, \quad U = V = 0 \quad \text{and} \quad I^* = I^*_\infty . \end{aligned} \tag{4}$$

When uniform suction is applied to the wall, the boundary conditions are

$$\begin{aligned} &\text{at } y = 0, \quad U = 0,\ V = V_w \quad \text{and} \quad I^* = I^*_w; \\ &\text{at } y \to \infty, \quad U = V = 0 \quad \text{and} \quad I^* = I^*_\infty . \end{aligned} \tag{5}$$†

The case of strip suction was also examined and will be described later.

The turbulent momentum transport term, $\overline{u'v'}$ in Eq. (2), is modeled using the concept of eddy diffusivity:

$$\overline{u'v'} = -\varepsilon_M \frac{\partial U}{\partial y} . \tag{6}$$

The turbulent energy transport term, $\overline{i^{*\prime}v'}$ in Eq. (3), is modeled by the concepts of a turbulent Prandtl number and an eddy diffusivity for energy.

$$Pr_t = \varepsilon_M / \varepsilon_H . \tag{7}$$

The momentum eddy diffusivity is determined differently in the inner and outer regions of the boundary layer. Near the wall a Prandtl mixing-length model (PML) is used,

$$\varepsilon_M = \ell^2 \left| \frac{\partial U}{\partial y} \right| , \tag{8}$$

with a mixing length proportional to the distance from the wall,

---

† For suction V_w will be a negative value

$$\ell = \kappa y \quad . \tag{9}$$

To model the viscous sublayer immediately adjacent to the wall, the Van Driest damping function is applied to the mixing length,

$$\ell = \kappa y D \tag{10}$$

where

$$\begin{aligned} &y^+ < A^+, \quad D = 1.0 - \exp\left[-y^+(\gamma_o/\gamma)/A^+\right] \ ; \\ &y^+ > A^+, \quad D = 1.0 \ . \end{aligned} \tag{11}$$

In the outer wall region, eddy diffusivity is determined by a one-equation turbulence kinetic energy model(TKE). The equation for turbulent kinetic energy is

$$\rho U \frac{\partial (q^2/2)}{\partial x} + \rho V \frac{\partial (q^2/2)}{\partial y} = -\rho \overline{u'v'} \frac{\partial U}{\partial y} - \mathcal{D} + \frac{\partial J_q}{\partial y} \ . \tag{12}$$

The production of kinetic energy is modeled by

$$-\rho \overline{u'v'} \frac{\partial U}{\partial y} = \rho \, \varepsilon_M \left(\frac{\partial U}{\partial y}\right)^2, \tag{13}$$

the dissipation by

$$\mathcal{D} = \rho b \left(q^2/2\right)^{3/2} \ell^{-1}, \tag{14}$$

and the diffusion by

$$J_q = \rho(\nu + \varepsilon_q) \frac{\partial (q^2/2)}{\partial y} \quad . \tag{15}$$

The eddy diffusivity for momentum and for kinetic energy are calculated from the turbulence kinetic energy by the following relationships:

$$\varepsilon_M = a\ell \left(q^2/2\right)^{1/2} \tag{16}$$

and

$$Sc_q = \varepsilon_M/\varepsilon_q \ . \tag{17}$$

The mixing length in the outer region is proportional to the boundary layer size.

$$\ell = \lambda\delta \tag{18}$$

The recommended value for Sc_q in Reference 1 is 1.7. The constants κ, A^+, a, b, and λ in Eqs. (9)-(16) were chosen as 0.41, 25.0, 0.5, 0.125, and 0.09, respectively.[1,12] A turbulent Prandtl number of 0.85 was used in the outer region of the boundary layer ($y^+ > 15.0$), and 1.7 in the inner region ($y^+ < 15$). This model for Pr_t is discussed in Reference 1.

Two important modifications were made to STAN-5 so the equations for the natural convection could be solved. These were needed because the code was set up to solve forced convection or mixed convection heat transfer problems, not pure natural convection problems. The first change was to add a transition criterion for transition from laminar to turbulent flow in natural convection. The criterion chosen was patterned after the momentum Reynolds number criterion used in STAN-5 for transition in forced convection. A momentum-type Reynolds number for a natural convection boundary layer was calculated based on the boundary layer thickness and the maximum velocity in the boundary layer. A value of 870 was selected for this Reynolds number. This results in transition on a vertical plate at the location noted experimentally for isothermal plates in air. That position corresponds to a Grashof number of about 7×10^9. This criterion for transition was chosen mainly because little or no information was found in the literature on transition in natural convection.

The other change made involved the location of the line dividing the regions where the PML and TKE models are used. As originally written, STAN-5 used the PML model for $y^+ \leq 2A^+$ and the TKE model for $y^+ > 2A^+$. This

dividing line could not be used for free convection since $2A^+$ is outside of the point of peak velocity in the natural convection boundary layer at moderate Grashof numbers, 10^9 - 10^{13}, resulting in an eddy viscosity of zero at the peak velocity. This is caused in the PML model by the zero mean velocity gradient at the peak velocity. Instead of using $y^+ = 2A^+$ as the dividing line, it was put at a value of y^+ equal to one fourth of the distance between the wall and the point of peak velocity in the boundary layer. This dividing line was used until it exceeded $2A^+$, after which a value of $2A^+$ was used. This occurs when the local Grashof number reaches a value of about 10^{13}. The model results in a laminar sublayer that is smaller than would exist in a forced convection flow after transition to turbulence and that grows to a normal forced convection sublayer at Grashof numbers greater than 10^{13}.

The justification for this change came from two previous works. The first work, by Lock and Trotter[5], cast serious doubt on the idea that the laminar sublayer in a natural convection boundary layer on a vertical surface for modest Grashof numbers ($Gr < 10^{10}$) is similar to the forced convection laminar sublayer. This work shows that large scale turbulence structures penetrated very close to the wall and the laminar sublayer, if it exists, must be smaller than for forced convection. This indicates the TKE model could be used closer to the wall than Reference 1 stated was appropriate in STAN-5. The restriction not allowing the TKE model to be used close to the wall in STAN-5, existed because no provisions were made for modifying the length scales of turbulence production and dissipation in Eqs. (11) and (12) in the sublayer near the wall for forced convection. But based on the work of Lock and Trotter this is probably not necessary at moderate Grashof numbers for natural convection, since the sublayer appears to be smaller, and therefore the TKE model can be used closer to the wall without modification.

The other work lending justification to the model is by Kato et al.[6] Their work shows that the boundary layer structure approaches that of forced convection for Grashof numbers greater than 10^{13}. Between transition to turbulence and a Grashof number of 10^{13}, the normal laminar sublayer assumption, $u^+ = y^+$ for $y^+ < 4$, is not appropriate. The closer the local Grashof number is to the transition value, the smaller the region in which $u^+ = y^+$ applies, which means the smaller the laminar sublayer.

Method of Solution

The method of solution used in STAN-5 is to recast the continuity momentum and energy equations into stream function coordinates using the von Mises transformation. The resulting equations are finite differenced. A fully implicit scheme is used for the main dependent variables -- velocity, enthalpy, etc. The fluid properties and turbulence properties are handled explicitly. For the details of the solution Reference 1 should be consulted.

Results and Discussion

The results of the numerical study are presented in Figures 1 through 7. The first three figures compare the numerical predictions of STAN-5 to other experimental, analytical, and numerical results for natural convection heat transfer at moderate Grashof numbers on vertical, uniform-temperature plates. The next two figures present STAN-5 predictions of heat transfer at high Grashof numbers in the range of interest for receivers of the solar central receiver concept. The final two figures present results showing the effects of wall suction on free convection heat transfer from a vertical plate. This form of boundary control could be a means of reducing convective losses from receivers.

The heat transfer is presented in terms of either local or average Nusselt number divided by the cube root of Prandtl number versus local or average Grashof number. The reference temperature used is the average of the wall and free stream temperatures.

Figure 1 compares the numerical predictions of heat transfer by STAN-5 to the experimental works of Saunders[7] and Warner and Arpaci[8] for moderate Grashof numbers. The experimental conditions were closely simulated in the numerical calculations. The results show that in both the laminar ($Gr < 5 \times 10^9$) and turbulent ($Gr > 5 \times 10^9$) ranges the numerical predictions of local heat transfer agree reasonable well with best fit curves for the various experimental results. Figure 2 is a comparison of the STAN-5 numerical predictions of heat transfer with the analytical works of Ostrach[9], Bayley[10], and Eckert and Jackson[11] and the numerical predictions of Mason and Seban[12] and Lin and Churchill[13]. The agreement of these works with STAN-5 is similar to that with the experimental results shown in Figure 2, with a

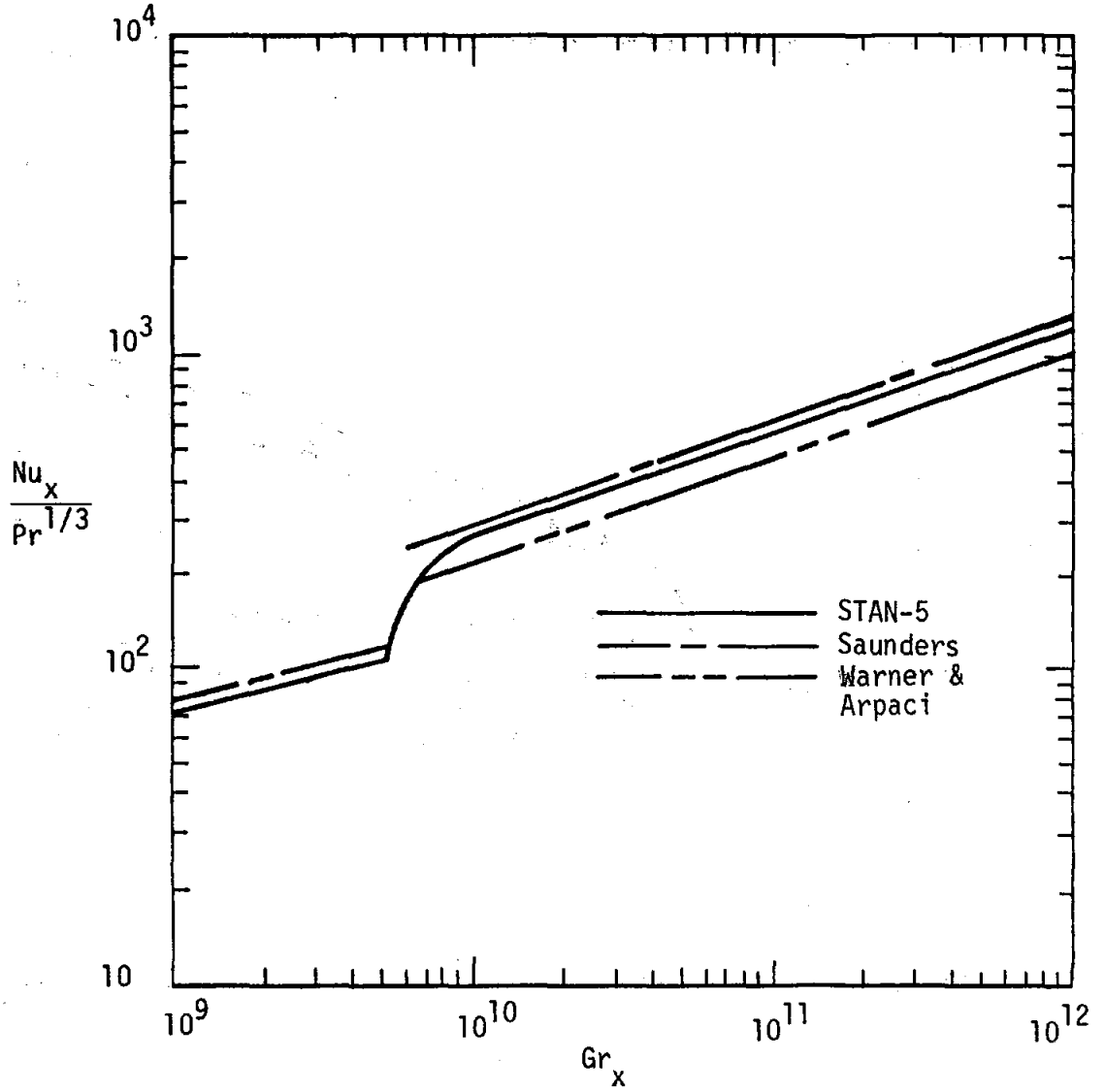

Figure 1. Comparison of Local Free Convection Heat Transfer Predictions With Previous Experimental Work.

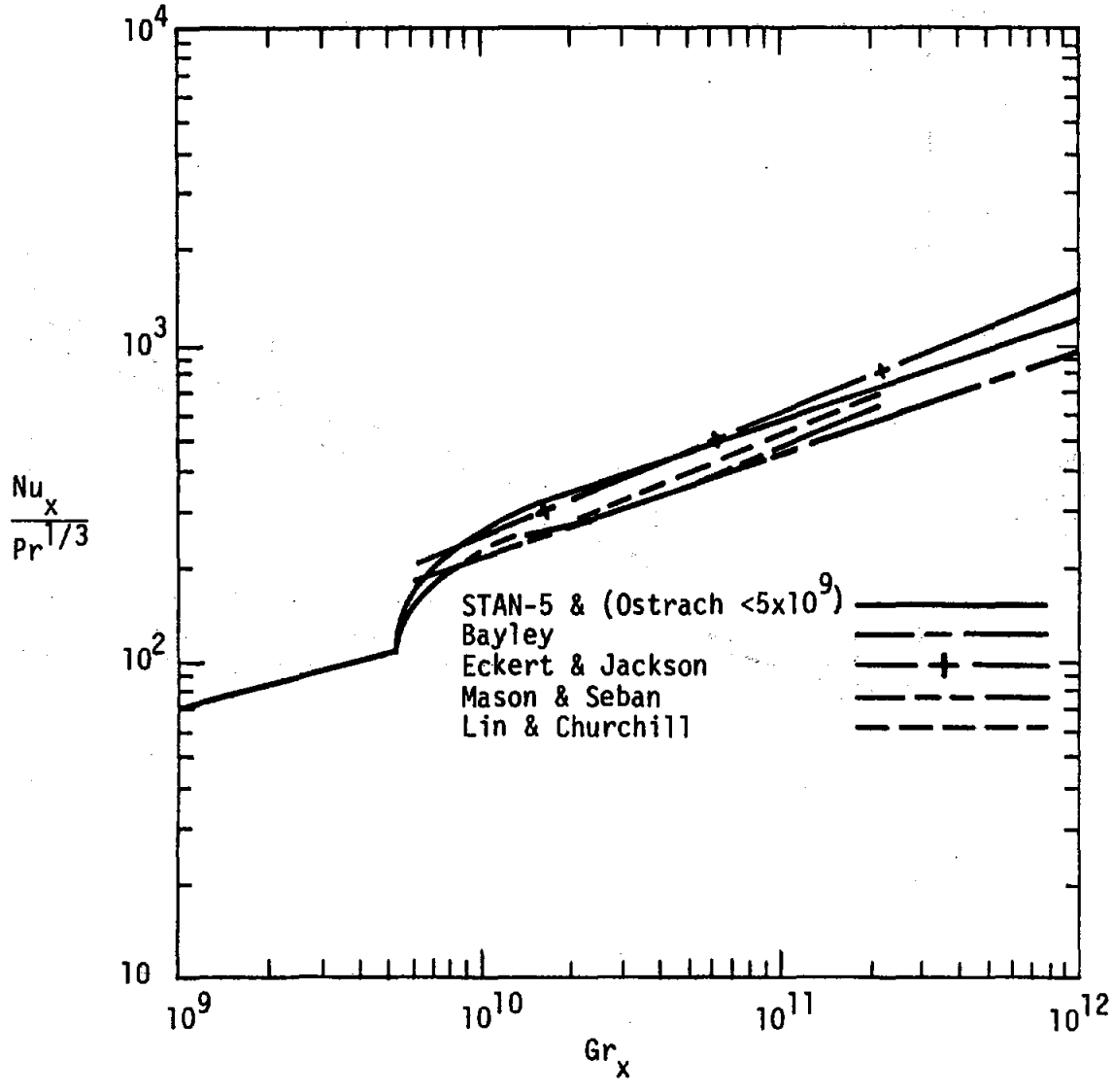

Figure 2. Comparison of Local Free Convection Heat Transfer Predictions With Previous Numerical and Analytical Work.

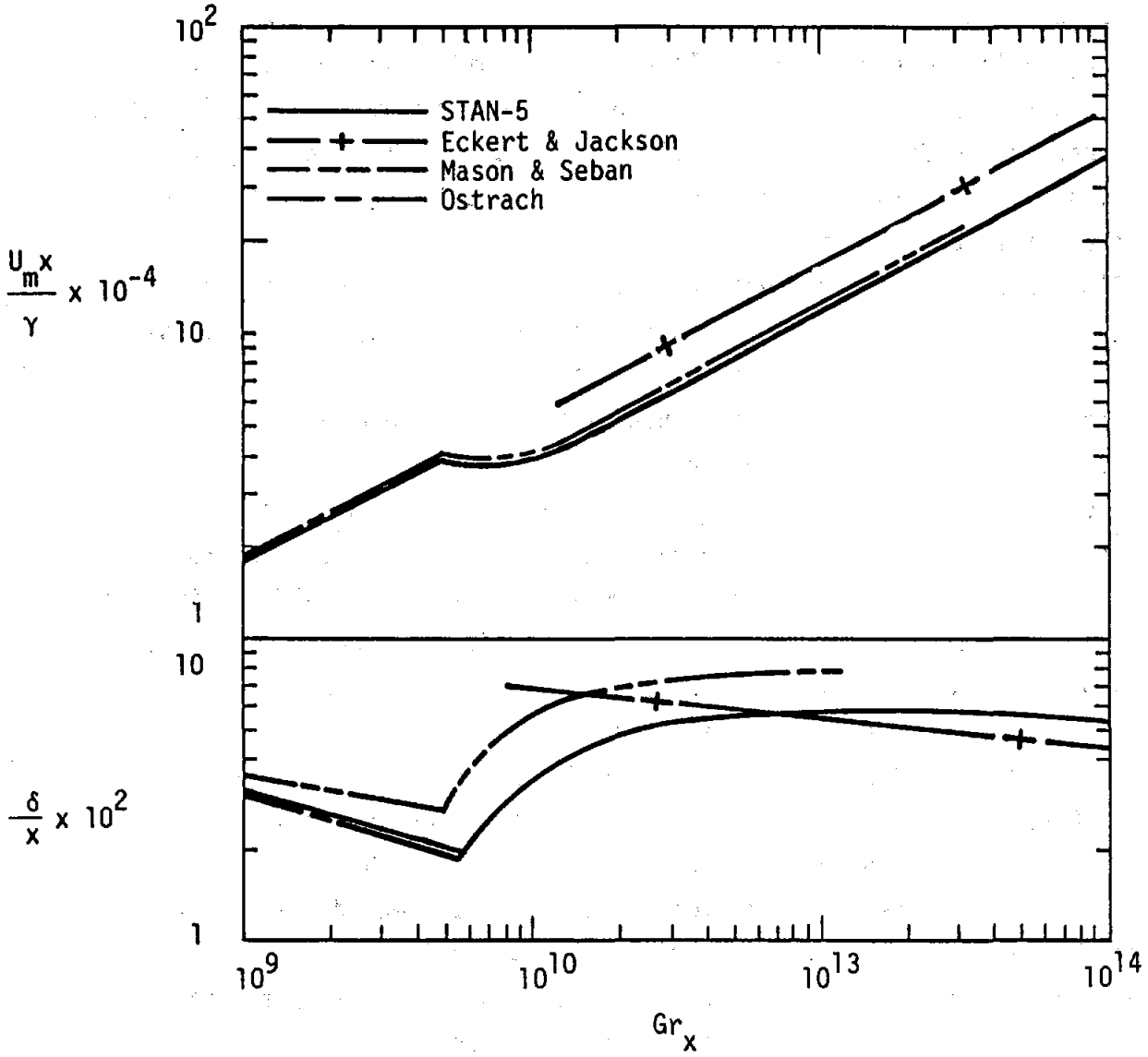

Figure 3. Comparison of Predicted Boundary Layer Size and Maximum Velocity with Previous Numerical and Analytical Work.

scatter of about 30% in the various data in both figures. Figure 3 presents a comparison of STAN-5 predictions of peak velocity in the boundary layer, expressed as $U_m x/\nu$, and the boundary layer size, expressed as δ/x, with a numerical and an analytical prediction of those same quantities. The peak velocity from STAN-5 agrees very well with the numerical prediction of Mason and Seban[12]. The trends in boundary layer size agree well also, but the magnitudes are different. This is believed to be the result of differing definitions of boundary layer size or differing entrainment calculations at the edge of the boundary layer in the two works, but this could not be determined for sure. The analytical results of Ostrach[9] agree in the laminar range. In the turbulent range the results agree in trend only with the analytical results of Eckert and Jackson[11].

Figures 1 through 3 demonstrate that the model used in this work for predicting heat transfer from a vertical smooth surface by natural convection is reasonable. Predictions agree with other experimental, analytical, and numerical results in the literature in both trend and magnitude of heat transfer and other important parameters.

The next two figures show one of the main interests of this work, a prediction of heat tranfer for the high temperatures and the high Grashof numbers that occur on a receiver. Figure 4 is a plot of local Nusselt versus local Grashof number predicted by STAN-5 for surfaces at 30 C and 530 C. Also shown are extrapolations of the analytical correlations of Eckert and Jackson[11] and Baley[10] and the experimental correlation given in McAdams[14] for lower Grashof numbers. The figure points out several facts. First, high temperature has a strong effect on the heat transfer in the boundary layer. There is about a 50% difference in heat transfer between the low and high temperature predictions of STAN-5. Second, extrapolation of McAdams' experimental correlation from the range of Grashof numbers in which the experiments were conducted appears to be conservative in predicting heat loss from a receiver at high temperatures. This correlation, the one most commonly used for predicting the natural convective component of heat loss from receivers by various designers, would result in heat transfer estimates 50 to 100 percent lower than the high temperature STAN-5 prediction in the Grashof number range of interest, 10^{13} - 10^{14}. Finally, the analytical results of Eckert and Jackson[11] fall somewhere inbetween the high and low temperature STAN-5 results. Figure 5 shows the average Nusselt versus average Grashof

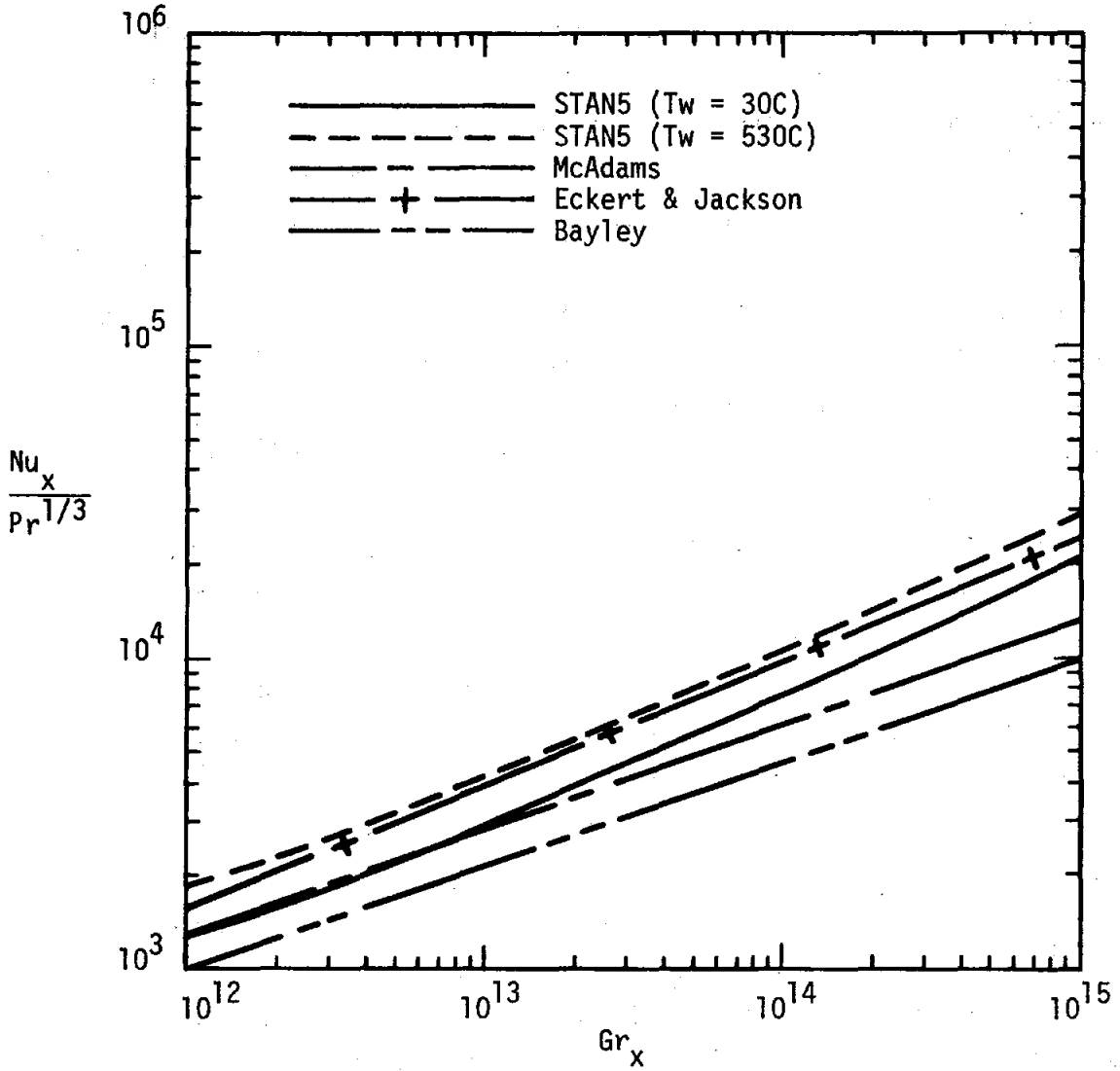

Figure 4. Local Free Convection Heat Transfer at High Grashof numbers.

number compared with other works. The results are similar to those in Figure 4. Also shown is the theoretical prediction of average heat transfer developed by Le Fevre.[15] This analytical expression applies as Grashof number approaches infinity. These results agree reasonably well with STAN-5's high temperature average heat transfer prediction.

These last two figures show that McAdams' correlation, based on experimental results at low Grashof number ($< 10^{12}$), may be conservative by a factor of 1.5 to 2.0. Also, the high temperatures that the receivers operate at have a significant effect on the heat transfer. This is probably the result of property variations across the boundary layer at high temperatures. The effect appears to be greater than the high-temperature effect noted in forced convection. In forced convection the increase in heat transfer caused by temperature is approximately $(T_f/T_a)^{0.14}$. The natural convection high and low temperature cases in Figures 4 and 5 differ by $(T_f/T_a)^{0.22}$. This added effect should be expected, since the temperature difference is the driving force for fluid motion in natural convective flow, unlike forced convection. As a result, any enhancement of heat transfer because of a temperature effect on properties would have a secondary effect of enhancing heat transfer by increasing the driving force (more hot fluid rising). This large effect also means that the assumption of constant properties across a boundary layer used to develop the analytical expressions for natural convection is not valid for natural convection with large temperature differences.

The next two figures present the results of the study of the effect of wall suction on natural convection heat transfer from a vertical plate. They show the heat loss from the wall and the energy extracted through the wall versus the suction rate at the wall. The heat loss at the wall, Q_w, is defined as the sum of the energy lost into the boundary layer, Q_{bl}, and the enthalpy of the fluid extracted through the wall, Q_s, which is assumed to be at the wall temperature. The heat transfer rates Q_w and Q_s are normalized with respect to Q_w with no suction applied. A wall at 530 C, 100 feet high, and ambient air at 30 C, were assumed for this study. These are representative of various receiver designs currently proposed.

Figure 6 is for uniform suction. The curve labeled zero is a plot of wall heat loss versus suction rate assuming all the fluid extracted through the wall is disgarded and not used. If this is done the figure shows that heat loss from a receiver by natural convection will increase with

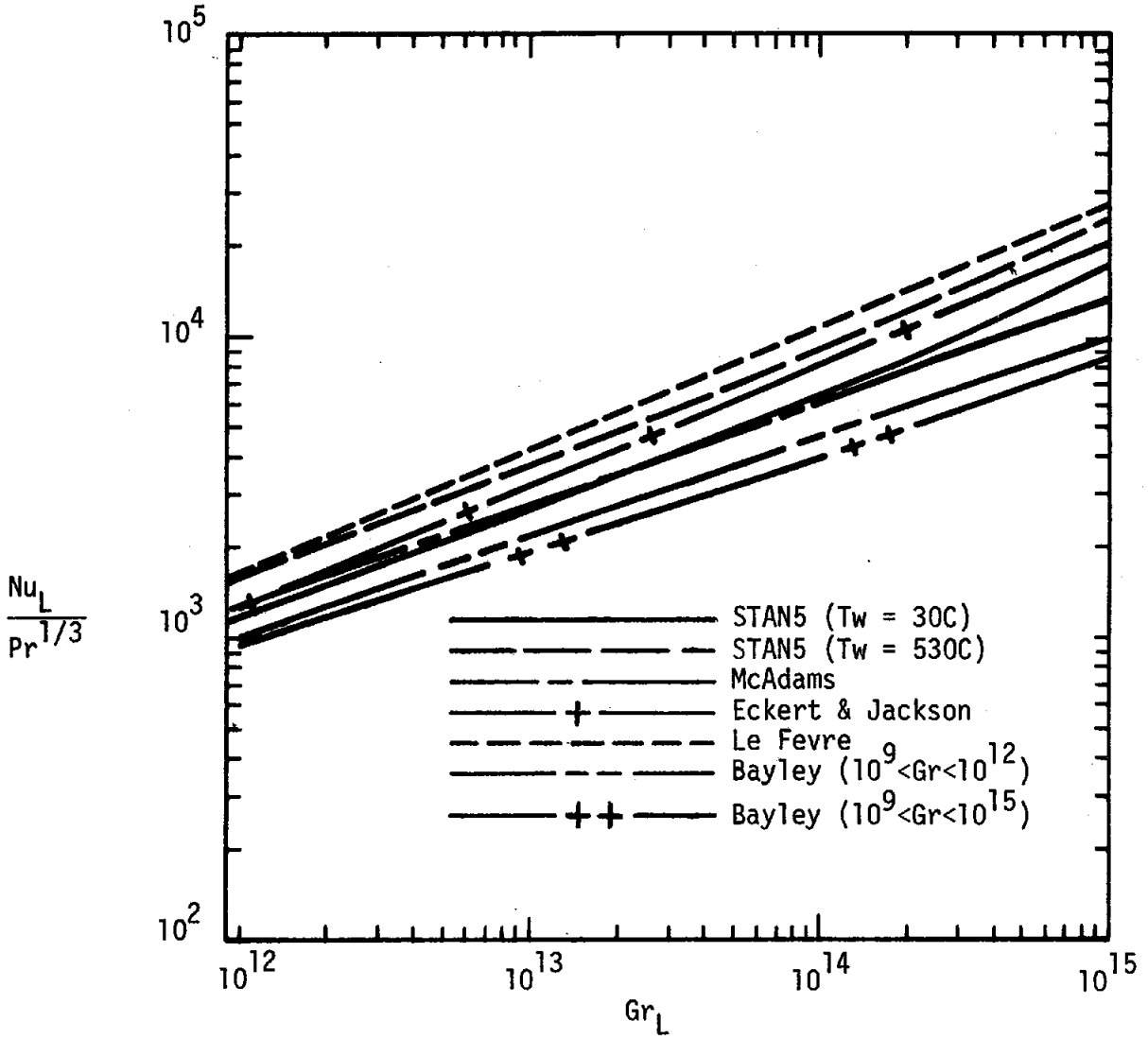

Figure 5. Average Free Convection Heat Transfer at High Grashof Numbers.

increasing suction rate until a suction of around 0.0018 lbm/ft^2/ sec is reached. After this the heat lost from the wall becomes very nearly equal to the energy extracted through the wall. What has happened is that more and more of the boundary layer on the plate remains laminar as the suction rate increases. At values of suction rate greater than 0.0019, the boundary layer is laminar over the entire plate. The heat loss to this laminar boundary layer is very small. The main heat lost from the wall is the energy extracted through the wall in the suction air. The figure shows there is a range of suction rates for which the heat lost from the wall is less than if no suction were applied. This range is between an $\dot{m}$ of 0.0019 to 0.0024. At an $\dot{m}$ of 0.0019 there is about 25% less heat transfer from the wall than with no suction. For the range of suction rates where the boundary layer is laminar, the boundary layer approaches an asymptotic state discussed in the literature.[16,17] The heat transfer predicted in this state agrees with analytical solutions presented in the literature.

On Figure 6 are two more curves labeled 40 and 80. These two curves represent the energy lost from a receiver if either 40 or 80 percent of the energy in the air extracted through the wall is used to preheat the working fluid flowing through the receiver wall before it enters the receiver. The curves show that the range of suction rates that can be applied to reduce the convection heat loss from a receiver increases as more of the energy in the suction fluid is used. As a matter of fact, if all the energy extracted through the wall in the suction fluid could be used to preheat the working fluid and the suction rate were high enough to insure laminar flow in the boundary layer, only the very small amount of energy carried away by the laminar boundary layer would be lost.

Since it might not be possible to apply uniform suction to a receiver, the case of strip suction was examined. These results are shown in Figure 7. The configuration studied was a vertical plate with the same temperature and length described for Figure 6, but with horizontal strips of suction rather than uniform suction. Suction strips of various widths and uniform distances apart were used. The representative curves shown are for suction strips of one foot width every three feet vertically, one foot width every ten feet vertically, and three foot width every ten feet vertically. The suction rate plotted in Figure 7 is an average suction rate. This is the suction rate obtained by taking the total fluid extracted through all the strips of

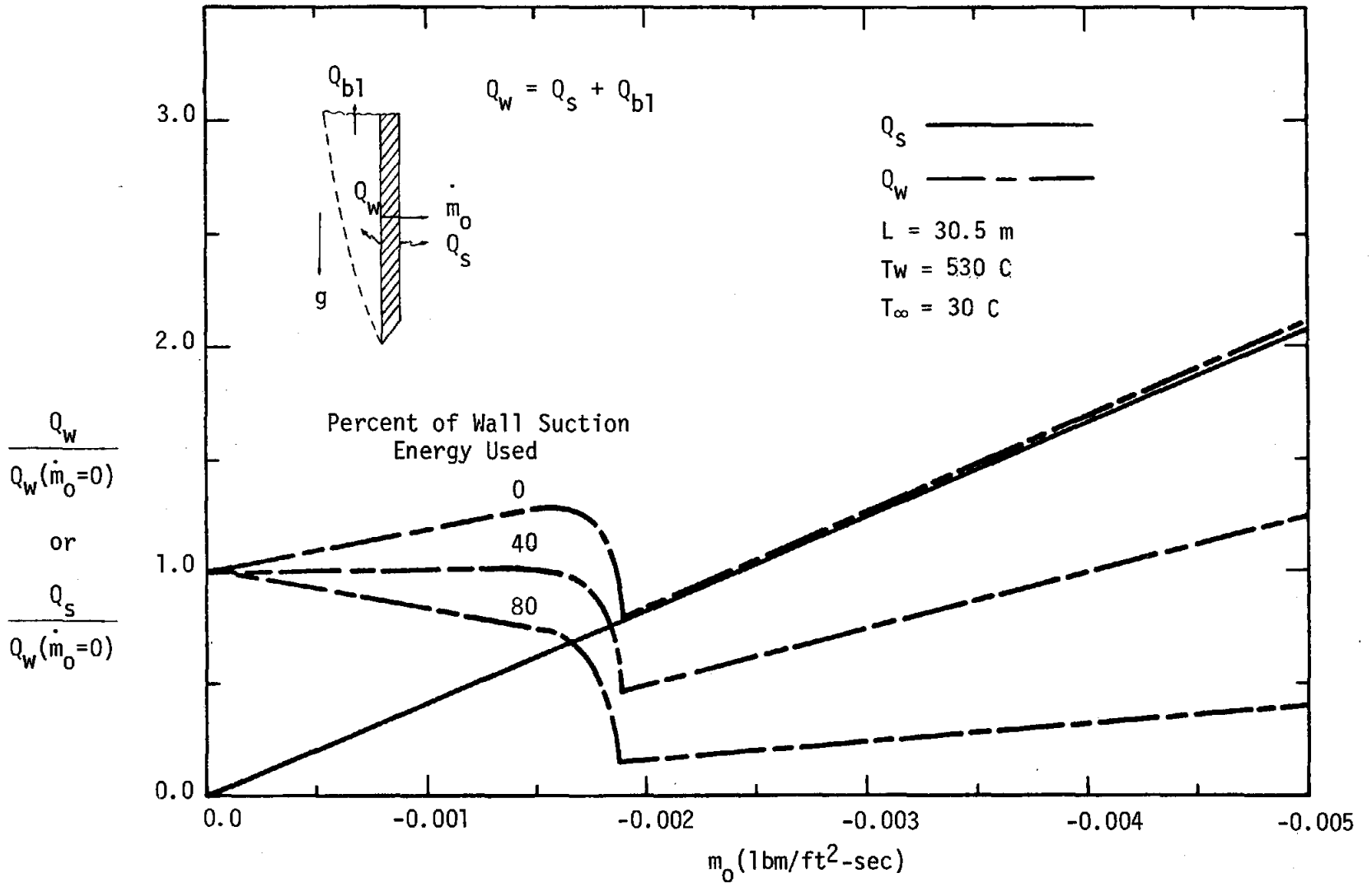

Figure 6. Effect of Wall Suction on Heat Transfer to the Free Convective Boundary Layer.

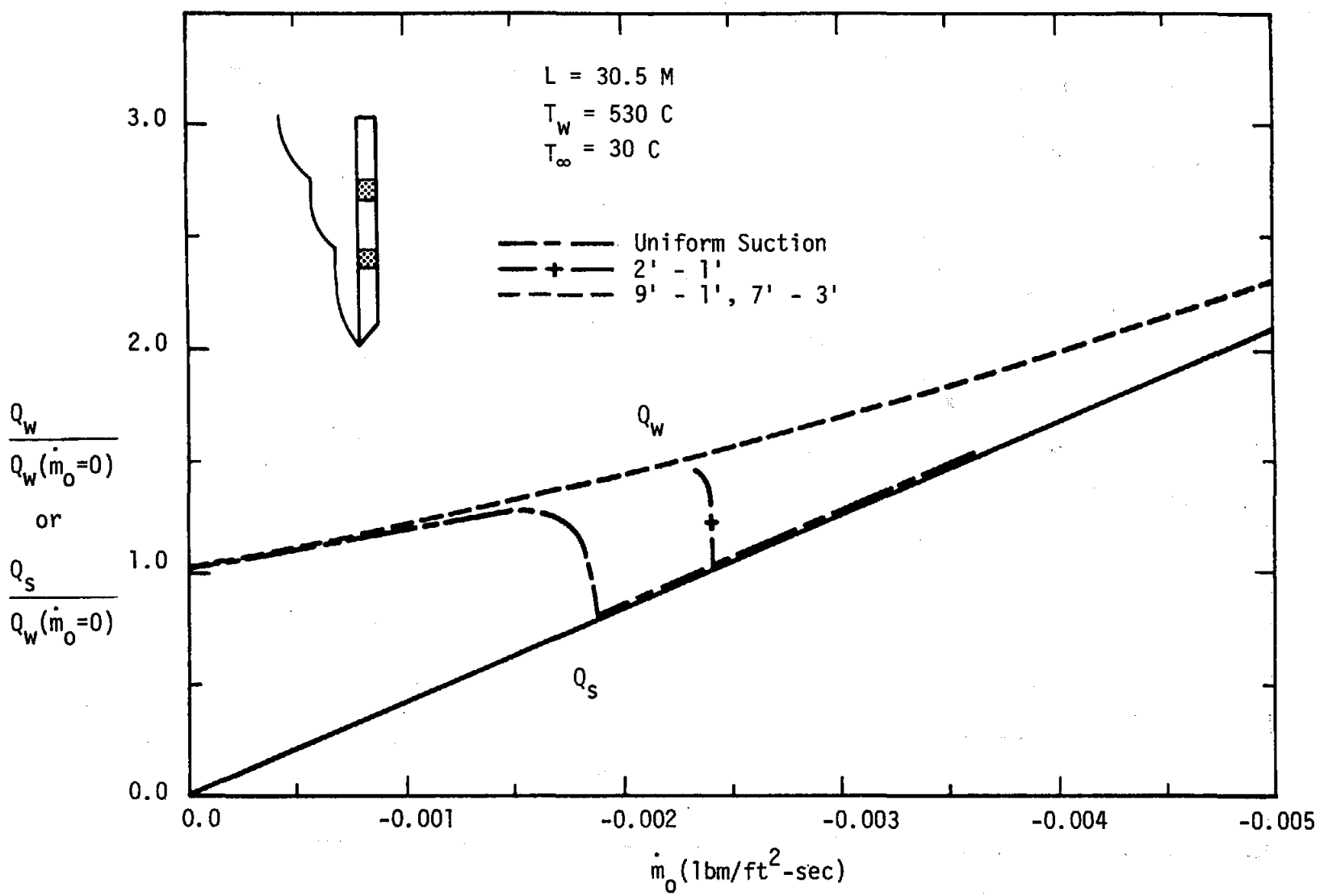

Figure 7. Effect of Strip Suction on Heat Transfer to the Free Convective Boundary Layer.

suction and averaging it over the entire plate area. In other words, this is the uniform suction which would have to be applied to the entire plate to extract the same amount of fluid through the wall as the strips of suction would.

The cases falling on the dashed line in Figure 7 are all those where the suction strips were further apart than the vertical distance required for the boundary layer to become turbulent (3' - 4'). This dashed line also happens to be the curve for heat loss from a wall if the boundary layer were constrained to be turbulent at all times. The strip suction cases fell on this line because, when no suction is applied before the boundary layer transitions to turbulent flow, a very high suction rate has to be applied to relaminarize the flow. A suction rate for this case is far to the right on the dashed curve in Figure 7 where, even for turbulent flow, the curves for Q_s and Q_w merge. For the case where a one-foot suction strip was applied every three feet, the flow could be made laminar over the entire length of the plate for values of average suction greater than 0.0024. There is no explanation for this average suction being greater than the minimum suction required to keep the flow laminar in the uniform suction case. Also shown in Figure 7 is the uniform suction case for comparison to strip suction.

Conclusion

Natural convection heat transfer caused by high operating temperatures and long vertical surfaces is important to receivers for the solar central receiver concept. The heat transfer correlations currently used to predict this high temperature, high Grashof number (10^{13} - 10^{14}) natural convection heat transfer are based on experimental work at much lower temperatures and Grashof numbers ($< 10^{12}$). The predictions using the model for natural convection heat transfer presented in this work cast serious doubt on the extrapolation of those experimental correlations to high temperatures and high Grashof numbers. The model, which is based on realistic physical assumptions, estimates heat transfer rates 50 to 100 percent higher for temperatures and Grashof numbers in the range of interest to receivers. For higher Grashof numbers the difference becomes even greater. This has serious consequences for the plant performance and cost estimates made with existing correlations.

The model also demonstrates that large temperature differences between the wall and free stream significantly effect the heat transfer as a result of the large property variations across the boundary layer. This means that correlations anlaytically derived assuming constant properties across a boundary layer and experimentally derived correlations at low temperatures are not appropriate for the high temperature natural convection heat transfer on receivers.

The boundary layer suction results show suction can be used to reduce convective heat loss from a receiver especially if some of the energy in the air extracted through the wall can be used to preheat the working fluid in the receiver. If the air extracted through the receiver wall is used as the working fluid, the convective heat losses can potentially be reduced to zero. Strip suction rather than uniform suction over the entire receiver can also be used. However if this is done, the results indicate some of the energy in the suction air must be used. Otherwise, the convection heat loss from the receiver would be greater for all suction rates.

Recommendations

In trying to develop a model for the natural convection boundary layer, the need for basic information on the structure of the turbulent natural convection boundary and on transition to turbulence in the natural convection boundary layer was discovered. This information is necessary for verification of the model used in this study or to help develop an improved model. Experiments and analysis should be carried out to help define a model for transition to turbulence in natural convection and for turbulence in flows up to Grashof numbers of about 10^{14}.

The concept of suction applied to a boundary layer should be examined experimentally and numerically in more detail than this work did. A realistic model of suction, taking into consideration the cost penalties of energy losses from a receiver on overall plant costs, can have a potentially large economic payoff for the solar central receiver. It can potentially provide the means for solving the convective loss problem from receivers by eliminating convective losses.

REFERENCES

1. Crawford, M. E. and Kays, W. M., "STAN5 - A Program for Numerical Computation of Two-Dimensional Internal and External Boundary Layer Flows," NASA CR-2742 (1976).
2. Kreith, J., Principles of Heat Transfer, 3rd ed., INTEXT, New York, 1973.
3. Gebhart, B., Heat Tranfer, 2nd ed., McGraw Hill, New York, 1970.
4. Schlichting, H., Boundary-Layer Theory, 6th ed., McGraw Hill, New York, 1968.
5. Lock, G. S. H. and Trotter, F. J. deB., "Observations on the Structure of a Turbulent Free Convection Boundary Layer," IJHMT 11, pp 1225-1232 (1968).
6. Kato, H., Nislwaki, N., and Hirata, M., "On the Turbulent Heat Transfer by Free Convection from a Vertical Plate," IJHMT 11, pp 1117-1125 (1968).
7. Saunders, O. A., "The Effect of Preessure Upon Natural Convection in Air," Proc. Royal Society 157, pp 278-291 (1936).
8. Warner, C. Y., and Arpaci, V. S., "An Experimental Investigation of Turbulent Natural Convection in Air Along a Vertical Heated Flat Plate," IJHMT 11, pp 397-406 (1968).
9. Ostrach, S., "An Analysis of Laminar Free-convection Flow and Heat Transfer About a Flat Plate Parallel to the Direction of the Generating Body Force," NACA TN 2635 (1952).
10. Bayley, F. J., "An Analysis of Turbulent Free-Convection Heat Transfer," Institution of Mechanical Engineers Proc. 169, No. 20, pp 361-370 (1955).
11. Eckert, E. R. G., and Jackson, T. W., "Analysis of Turbulent Free-Convection Boundary Layer on Flat Plate," NACA 1015 (1951).
12. Mason, H. B. and Seban, R. A., "Numerical Predictions for Turbulent Free Convection From Vertical Surfaces," IJHMT 17, pp 1329-1326 (1974).

13. Lin, Shyy-Jong and Churchill, S. W., "Turbulent Free Convection from a Vertical, Isothermal Plate," Numerical Heat Transfer 1, pp 129-145 (1978).
14. Mc Adams, W. H., Heat Transmission, McGraw-Hill, New York (1954).
15. Le Fevre, E. J. Proc. 9th Intern. Cong. Oppl. Mech., Brussels 4, 168 (1956).
16. Eichhorn, R., "The Effect of Mass Transfer on Free Convection," JHT 82, p 260 (1960).
17. Pande, G. C., Georgantopoulos, G. A., and Goudas, C. L., "Free Convection Effects on the Unsteady Laminar Boundary-Layer Flow Past a Proous Limiting Surface with Uniform Suction in Stellar Atmospheres," Astrophysics and Space Science 60, pp 125-171 (1979).
18. "The Cost of Energy from Utility-Owned Solar Electric Systems - A Required Revenue Methodology for ERDA/EPRI Evaluations," JPL5040-29 and ERDA/JPL-1012-76/3, Pasadena, CA, June 1976.
19. Brune, M. J., "Bucks - Economic Analysis Model of Solar Electric Power Plant," SAND77-8279.
20. "Recommendations for the Conceptual Design of the Barstow, California, Solar Central Receiver Pilot Plant - Executive Summary," SAND77-8035.

APPENDIX--EFFECT OF RECEIVER EFFICIENCY ON SOLAR CENTRAL RECEIVER CAPITAL AND ENERGY COSTS

Models expressing the sensitivity of the plant capital cost and energy cost to receiver efficiency are developed for a solar-thermal power plant. Before presenting those models a brief summary of the methodology used to calculate energy costs will be presented. A complete description of the methodology can be found in Reference 18. It is the method used by Sandia Laboratories in their evaluation of Solar Large Power Systems.[19]

The approach used to calculate energy costs in Reference 18 is to determine an energy "price" necessary to charge in order that all costs of purchasing, installing, and operating a solar-electric energy system are recovered in the life of a plant. In other words, it is the cost per unit of electrical energy produced that must be levied by a utility if the system is to break even. The costs to be recovered include, among other items, taxes and return on investments of bondholders and creditors, but exclude transmission and distribution costs.

The exact method used to calculate the energy cost (cost per unit of energy or busbar energy cost) is an annualized fixed charge approach. The resulting busbar energy cost is a levelized cost or average busbar cost which must be charged for the lifetime of the power plant. The relationship for calculating the levelized busbar energy cost is

$$\overline{BBEC} = \overline{AC}/KWH; \tag{A1}$$

$\overline{AC}$ is the charge which must be recovered annualy for the plant to break even; KWH is the annual energy output of the plant in kilowatt hours. These terms are calculated as follows:

$$\overline{AC} = \overline{FCR} \cdot CI \cdot d + \overline{OM} + \overline{FL}, \tag{A2}$$

$$KWH = CF \cdot CAP \cdot 8760, \tag{A3}$$

where

$$CI = C + RI + B \ . \tag{A4}$$

The annualized fixed charge rate is the fraction of the capital investment which must be recovered annually for the lifetime of the plant. It is a condensation of all utility description data into a single term. The term d is the factor for capital investment cost increase due to interest charged during the construction period. All costs are expressed in mills and the number 8760 is the number of hours in a year. Equations (A1)-(A4) give $\overline{BBEC}$ in mills per kilowatt hour, the standard units for $\overline{BBEC}$.

Assuming Eqs. (A1)-(A4) are valid, then relationships between receiver efficiency and capital cost and receiver efficiency and energy cost can be generated. To derive these relationships the following assumptions are made;

1. The power plant life is thirty years.
2. Only collector costs (through field size) and no others costs, are affected by receiver efficiency.
3. The collector field cost is inversely proportional to receiver efficiency,

$$C_n = \frac{C_{100}}{n} \ , \tag{A5}$$

   where C_{100} is the theoretical collector field cost for a plant with a 100 percent efficient receiver.
4. All heliostats in the field have the same performance.
5. The receiver thermal output and downstream power plant subsystems, turbine, storage, etc., are held constant; only the collector field size varies.

The first assumption is a common assumption for electric generating power plants. Assumption 2 is true for small perturbations in receiver efficiency (5%-10%). The third and fourth assumptions are conservative (under predict sensitivity), since any improvement in receiver efficiency

would result in subtracting heliostats from the outer edge of the field, where the heliostats are less efficient in directing energy to the receiver. This means more heliostats would be removed for a receiver efficiency gain when looking at the local mirror field properties than the average field properties as this analysis does. An alternative to Assumption 5 is to hold the receiver input (the collector field size) and everything downstream, turbine, storage, etc., constant and let the receiver output vary. This analysis produces similar results with more difficulty and will not be presented here.

With these assumptions and Eqs. (A1)-(A5) the desired relationships can be developed. The sensitivity of energy cost to receiver efficiency is simply the derivative of Eq. (A1) with respect to efficiency,

$$\frac{d\ \overline{BBEC}}{dn} = -\ (\overline{FCR} \cdot d \cdot C_{100}\ /KWH)\ \frac{1}{n^2} \cdot \qquad (A6)$$

If this is rearranged, the sensitivity of capital cost to receiver efficiency is developed,

$$\frac{d\$_c}{dn} = \frac{KWH}{\overline{FCR} \cdot d} \cdot \frac{d\ BBEC}{dn} = -\ C_{100}\ \frac{1}{n^2} \qquad (A7)$$

This equation also gives the maximum amount of capital which can be spent for a given plant to improve its receiver efficiency a certain amount and still produce power for the same cost.

Another energy cost relationship which can be developed from Eq. (A6) is the added cost or savings to the public over the thirty year plant life due to a change in receiver efficiency. This is developed by multiplying Eq. (A6) by the annual energy output of the plant and a present worth factor to give the dollar cost or savings for the thirty year plant life:

$$\frac{d\$_e}{dn} = -\ (\overline{FCR} \cdot C_{100} \cdot d \cdot PW)\ \frac{1}{n^2} \qquad (A8)$$

If an $\overline{FCR}$ of 0.18, a d of 1.2, and PW of 19.6, are assumed,† then Eq. (A8) becomes

$$\frac{d\$_e}{dn} = -4.2 \cdot C_{100} \cdot \frac{1}{n^2} . \qquad (A9)$$

Figure A1 is a plot of Eq. (A9) assuming a receiver efficiency of 90%. Three different heliostat costs are used, which range from the most optimistic of \$70/m^2 to a very high cost of \$180/m^2. The graph indicates the receiver has a significant cost impact. It also shows the potential savings which can be obtained by improving receiver efficiency. For example, the commercial plant design as recommeded in Reference 19 is shown in Figure A1. This is a plant with a collector field cost of 107 million dollars. The $\frac{d\$_e}{dn}$ at the design efficiency of the receiver is \$5.2 x 10^8/unit efficiency. If the efficiency were improved 1.0 percent the savings would be 0.01 times this number or \$5.2 x 10^6 over the thirty year plant life assuming only minor changes in the receiver cost are needed to achieve that efficiency gain.

The cost analysis graphically shows the potential savings which can be achieved through design of more efficient receivers. In addition to that it demonstrates the potential cost of an error in evaluating the receiver efficiency. The results indicate significant effort should be placed on improving our receiver efficiency evaluating capability, as well as on research aimed at finding methods of improving receiver efficiency.

† Other fixed charge rates, etc., could be used, but these correspond to a reasonable economy, one that has a discount rate of 11% and an inflation rate of about 8% for an effective discount rate of 3% or an $\overline{FCR}$ = 0.18.

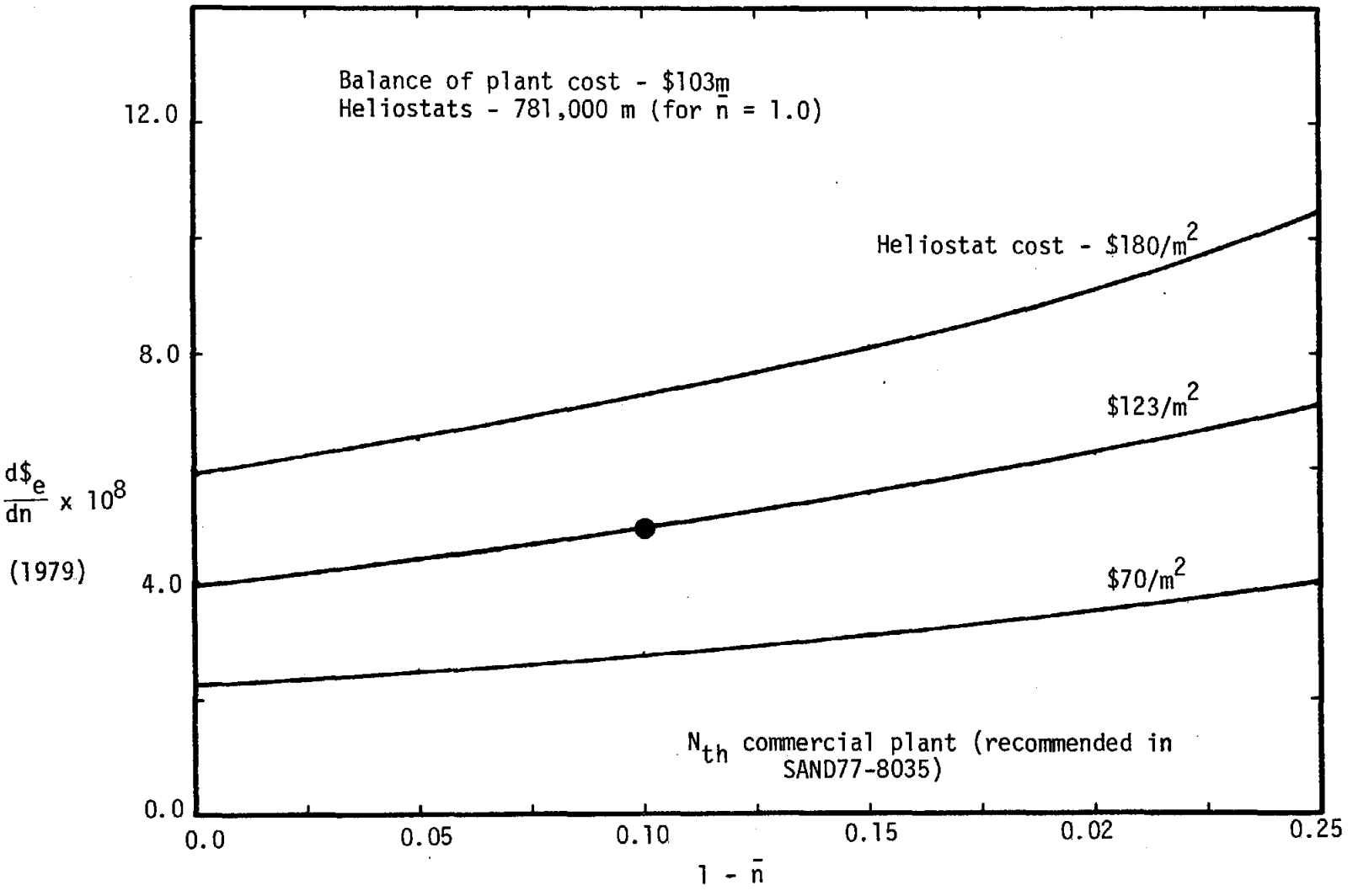

Figure A1. Sensitivity of Energy Cost of Receiver Efficiency.

UNLIMITED RELEASE
INITIAL DISTRIBUTION

Dan E. Arvizu
M.E. Dept.
Stanford University
Stanford, CA 94305

Thomas E. Bailey
Martin-Marietta Corp.
P. O. Box 179
Denver, CO 80201

Gerald C. Coleman
McDonnell Douglas Corp.
5301 Bolsa Ave.
Huntington Beach, CA 92647

Roger Eichhorn
University of Kentucky
Lexington, KY 40506

Richard J. Goldstein
Mechanical Engineering Dept.
University of Minnesota
Minneapolis, NM 55455

Ralph Greif
Mechanical Engineering Dept.
University of California
Berkeley, CA 94720

Joseph A. C. Humphrey
Mechanical Engineering Dept.
University of California
Berkeley, CA 94720

Philip O. Jarvinen
MIT - Lincoln Lab. I-213
Box 72
Lexington, MA 02173

James P. Johnston
Mechanical Engineering Dept.
Stanford University
Stanford, CA 94305

Frank Kreith
Solar Energy Research Institute
1536 Cole Blvd.
Golden, CO 80401

Brian E. Launder
Mechanical Engineering Dept.
University of Calif. at Davis
Davis, CA 95616

Patrick LeQuere
Groupe de Projet THEM
D.E.R.
6 Quai Watier
78400 Chatou, FRANCE

Robert J. Moffat
Mechanical Engineering Dept.
Stanford University
Stanford, CA 94305

Joseph C. Mollendorf
Mechanical Engineering Dept.
State Univ. of NY at Buffalo
604 Furnas Hall
Amherst, NY 14217

Jack N. Nielsen
N.E.A.R. Inc.
510 Clyde
Mt. View, CA 94043

Simon Ostrach
Mechanical Engineering Dept.
Case Western Reserve University
University Circle
Cleveland, OH 44106

Armand R. Poirier
Sanders Associates Inc.
95 Canal St.
Nashua, NH 03060

Fredrick S. Sherman
Mechanical Engineering Dept.
University of California
Berkeley, CA 94720

HANS F. STERNFELD
DFVLR
LAMPOLDSHAUSEN - D-7101
WEST GERMANY

K. Touryan
Solar Energy Res. Institute
1536 Cole Boulevard
Golden, CO 80401

Raymond Viskanta
School of Mechanical Engineering
Purdue University
W. Lafayette, IN 47907

A. F. Baker
Beethovenallee 79-Corner
Vikloria Str.
53 Bopnn 2
W. GERMANY

Dr. Claude Etievant
CNRS/EDF Project Them
Direction des Estudes et Recherches EDG
6 Quai Watier
78 Chateau
FRANCE

Frank Smith
Solar Users Association
Suite 1204
First National Bank E
Albuquerque, NM 87108

General Electric ESPD
Schenectady, NY 12345
Attn: R. Salemme
T. Ku
R. H. Horton
S. Schwartz
J. Elsner
B. Pomeroy

Black & Veatch Consulting Engineers
P. O. Box 8405
Kansas City, NO 64114
Attn: J. T. Davis
S. L. Levy
Mike Wolf P5A1

Foster Wheeler Development Corp.
12 Peach Tree Hill Road
Livingston, NJ 07039
Attn: G. D. Gupta
R. J. Zoschak

Aerospace Corp.
P. O. Box 92957
Los Angeles, CA 90009
Attn: P. Mathur
E. L. Katz

Bechtel National, Inc.
P. O. Box 3965
San Francisco, CA 94110
Attn: R. L. Lessley 301-3
E. Y. Lam

University of Houston
Solar Energy Laboratory
4800 Calhoun
Houston, TX 77004
Attn: F. Lipps
L. Vant-Hull

J. E. Bigger
EPRI
P. O. Box 10412
Palo Alto, CA 94304

General Electric Co.
P. O. Box 8661
Philadelphia, PA 19101
Attn: M. A. Van Horn

Joseph N. Reeves
Southern California Edison
P. O. Box 800
Rosemead, CA 94770

Dynatherm Corpation
One Industry Lane
Cockeysville, MD 21030
Attn: D. Wolfe

Claudio A. Arano
Centro Estudios Energia
Agustin De Foxa 29
Madrid, SPAIN

Manfred Becker
DFVLR
Linder Hohe
5000 Cologne 90, GERMANY

A. M. Clausing
University of Illinois
266 Mech. Eng. Bldg.
Urbana, IL 61801

James W. Doane
Solar Energy Res. Institute
1536 Cole Blvd.
Golden, CO 80401

S. D. Elliott
Solar Energy Division
DOE/SAN Office
1333 Broadway
Oakland, CA 94612

J. C. Grosskreutz
Solar Energy Res. Institute
1536 Cole Blvd.
Golden, CO 80401

M. U. Gutstein
Division of Solar Technology
Department of Energy
Washington, D.C. 20545

Alvin F. Hildebrandt
Univ. of Houston
Solar Energy Laboratory
Houston, TX 77004

George M. Kaplan
Large Power Systems Branch
Division of Central Power Systems
Department of Energy
Washington, DC 20545

Dr. Lewis Leibowitz
Mail Stop 506-328
Jet Propulsion Laboratory
4800 Oak Grove Drive
Pasadena, CA 91003

Louis Melamed, Prog. Manager
Division of Solar Technology
Department of Energy
Washington, DC 20545

R. N. Schweinberg
DOE/STMPO
9550 Flair Park Drive
Suite 210
El Monte, CA 91731

John P. Thornton
Solar Energy Res. Institute
1536 Cole Blvd.
Golden, CO 80401

John P. Thornton
Solar Energy Res. Institute
1536 Cole Blvd.
Golden, CO 80401

Dr. Vincent Truscello
Jet Propulsion Laboratory
Mail Stop 502-201
4800 Oak Grove Drive
Pasadena, CA 91103

SERI
1536 Cole Boulevard
Golden, CO 80401
Attn: R. Copeland
D. Horgan
J. Doane
N. Woodley

M. Sparks
A. Narath, 4000
J. H. Scott, 4700
G. E. Brandvold, 4710
B. W. Marshall, 4713
V. L. Dugan, 4720
J. V. Otts, 4721
J. F. Banas, 4722
W. P. Schimmel, 4723
J. A. Leonard, 4725
A. C. Ratzel, 4512
B. W. Marshall, 4713
R. Stromberg, 4714
R. H. Braasch, 4715
T. B. Cook 8000; Attn: A. N. Blackwell, 8200
W. E. Alzheimer, 8120
C. S. Hoyle, 8122
R. J. Gallagher, 8124
D. Siebers, 8124 (10)
P. W. Dean, 8265
B. F. Murphy, 8300
J. Swearengen, 8316
T. S. Gold, 8320
P. J. Eicker, 8326
J. J. Iannucci, 8326
M. J. Fish, 8326
G. W. Anderson, 8330
R. J. Kee, 8331
R. E. Huddleston, 8332
D. Hartley, 8350
B. R. Sanders, 8354
L. Gutierrez, 8400
C. S. Selvage, 8420
R. C. Wayne, 8450

D. N. Tanner, 8450A
W. G. Wilson, 8451
T. A. Dellin, 8451
A. C. Skinrood, 8452
T. T. Bramlette, 8453
J. D. Gilson, 8453
F. J. Cupps, 8265

Technical Publications and Art Division, 8265 for TIC (27)
F. J. Cupps, 8265/Technical Library Processes Division, 3141
Technical Library Processes Division, 3141 (2)
Library and Security Classification Division, 8266-2 (3)